communications earth & environment

SCCWRP#1337

ARTICLE

https://doi.org/10.1038/s43247-023-00833-2 OPEN

Large global variations in the carbon dioxide removal potential of seaweed farming due to biophysical constraints

Isabella B. Arzeno-Soltero [1,2]✉, Benjamin T. Saenz [3], Christina A. Frieder[4], Matthew C. Long[5], Julianne DeAngelo [6], Steven J. Davis [1,6] & Kristen A. Davis [1,6]✉

Estimates suggest that over 4 gigatons per year of carbon dioxide (Gt-CO_2 year^{-1}) be removed from the atmosphere by 2050 to meet international climate goals. One strategy for carbon dioxide removal is seaweed farming; however its global potential remains highly uncertain. Here, we apply a dynamic seaweed growth model that includes growth-limiting mechanisms, such as nitrate supply, to estimate the global potential yield of four types of seaweed. We estimate that harvesting 1 Gt year^{-1} of seaweed carbon would require farming over 1 million km^2 of the most productive exclusive economic zones, located in the equatorial Pacific; the cultivation area would need to be tripled to attain an additional 1 Gt year^{-1} of harvested carbon, indicating dramatic reductions in carbon harvest efficiency beyond the most productive waters. Improving the accuracy of annual harvest yield estimates requires better understanding of biophysical constraints such as seaweed loss rates (e.g., infestation, disease, grazing, wave erosion).

[1] Department of Civil and Environmental Engineering, UC Irvine, Irvine, CA, USA. [2] Department of Civil and Environmental Engineering, Stanford University, Stanford, CA, USA. [3] biota.earth, Berkeley, CA, USA. [4] Southern California Coastal Water Research Project, Costa Mesa, CA, USA. [5] National Center for Atmospheric Research, Boulder, CO, USA. [6] Department of Earth System Science, UC Irvine, Irvine, CA, USA. ✉email: iarzeno@stanford.edu; davis@uci.edu

Recent analyses of global climate scenarios suggest that limiting warming to <1.5° above pre-industrial levels will require large reductions in greenhouse gas emissions as well as the removal of ~2.5–13 Gt-CO_2 $year^{-1}$ (~0.7–3.6 GtC $year^{-1}$) by midcentury[1,2]. Some strategies for reducing greenhouse gas emissions include incorporating farmed macroalgae (seaweed) into human and animal diets[3–5] or generating biofuels[6–8], though some challenges still limit the efficient production and commercial-scale use of seaweed-based biofuels[9]. While concurrently providing ecosystem services[10] or advancing the bioremediation of coastal waters[11–14], seaweed farming could also enhance ocean carbon dioxide removal (CDR) by fixing carbon from the surface ocean into organic biomass, which can subsequently be sunk to the deep ocean, or otherwise isolated from the atmosphere[15–18]. In contrast to terrestrial biomass, seaweed farming does not require arable land or freshwater. Indeed, the seaweed farming industry is growing: annual production of seaweed increased by an average of 13% between 2015 and 2020, with 3.5 Mt of dry weight (~1 MtC) harvested globally in 2020[19]. Although most farming today occurs in the coastal waters of China and Indonesia, technology to farm offshore is in development[20–24].

Early assessments of the global potential to farm seaweed, though noteworthy, have generally extrapolated from observed yields in high-nutrient regions[13,15–17,25] or average global biomass of wild seaweeds[5,26], neglecting spatial variations in hydrodynamics, nutrient fluxes, and uncertainty in seaweed productivity and aquaculture yields. Meanwhile, dynamic models of seaweed growth under nutrient and other environmental limitations[27–31] have often focused on relatively small (<500 km^2) coastal areas and have not examined the levels of intensive nutrient uptake required to produce biomass at scales relevant to the global carbon budget (e.g., >1 GtC). One recent study modeled macroalgal cultivation worldwide but focused on one seaweed group and did not explore biophysical uncertainties[32]. Here we develop and use a global dynamic model of seaweed growth, the Global MacroAlgae Cultivation MODeling System (G-MACMODS), to analyze the potential of seaweed farming to produce Gt-scale biomass carbon under assumptions of growth-limiting mechanisms. We focus on the offshore cultivation of four seaweed types and systematically test the sensitivity of seaweed harvested yield to a range of uncertain biophysical parameters.

Details of G-MACMODS, data sources, and analytical methods are in Methods. In summary, the model (Supplementary Fig. 1; informed by a previous macroalgae cultivation model[33]) predicts spatially-resolved (1/12th° resolution) cultivated seaweed yield with constraints from both extrinsic (environmental forcing) and intrinsic factors (biological parameters; e.g., growth rates, nitrate uptake, nitrogen exudation, and mortality, among others). To test sensitivities and evaluate uncertainties, we performed 1012–1066 simulations of macroalgal growth and harvest for each of four seaweed types (defined using biophysical characteristics from currently-farmed temperate and tropical red and brown genera). Each simulation sampled from a uniform distribution of parameter values spanning the full range of relevant values reported in the literature (Supplementary Table 1). Environmental forcing included water temperature, solar irradiance, current velocities, wave height, wave period, and nitrate concentrations, sourced from a combination of satellite measurements (MODIS) and global ocean model simulations (HYCOM and CESM). Although we tested the model with forcing data from different years, results reported here reflect the year 2017 (a recent year without strong El Niño/La Niña anomalies; Supplementary Figs. 2, 3) and a representative seasonally-varying climatology of physically-mediated nitrate fluxes (Supplementary Fig. 4). Simulations that use parameter values best supported by the literature or deemed the most appropriate by the authors are termed standard runs. Seeding and harvesting for each seaweed type were optimized based on the yields from this standard configuration. We assess the importance of different model parameters using "random forest" classification analysis.

G-MACMODS assumes that nitrogen is the limiting nutrient because its demand relative to other nutrients, such as phosphorus, is often greater than its supply in the ocean[34]. The average N:P ratio in macroalgae is 38:1[35], yet the median N:P ratio in the ocean is 22:1[36]. G-MACMODS specifically incorporates nitrogen in the form of nitrate, although other forms of nitrogen (e.g., ammonium and urea) can contribute to seaweed growth in low-nitrate environments[37,38]. Presuming that nitrogen is the only limiting nutrient is a potential shortcoming of the model framework, but we assume that other nutrient constraints (e.g., iron scarcity) can be overcome by farming practices.

We consider two bounding nitrate scenarios: (1) an ambient nitrate case in which average nitrate concentrations within the top 20 m are available to seaweed without depletion or competition and (2) a limited nitrate case where biomass accumulation is capped by that which is replenished daily through natural vertical fluxes of nitrate across 100-m depth (i.e., through mixing or upwelling). The ambient nitrate scenario, while unrealistically optimistic for intensive production on a global scale without artificial upwelling, is representative of the potential yield in a given area if the farming intensity is low and does not generate substantial feedback by modifying regional nitrate budgets. The ambient nitrate case applies to small seaweed cultivation farms such as those currently in operation in Indonesia (<1 ha[39]), the Philippines (<3 ha[40]), or Chile (<25 ha[41]). In contrast, the limited nitrate scenario may better reflect constraints under dense farming, such as seen in China (> 3500 ha[42]), or under conditions of phytoplankton competition[32,43]. In the limited nitrate scenario, we cap the nitrate available to seaweed to that which is replenished by natural vertical fluxes, since dense farms can limit nutrient resupply from surrounding waters by stifling the cross-shore exchange[44]. Both the ambient nitrate and the limited nitrate cases are idealized scenarios because the "offline" implementation of G-MACMODS does not explicitly account for feedback to nitrate cycling or competition with phytoplankton. The different scenarios are intended to help gauge the sensitivity of seaweed growth to nitrate constraints. Our analysis focuses on offshore production, under the assumption that competing uses of nearshore environments will preclude dramatic expansion of nearshore cultivation activities.

The purpose of this work is not to advocate for the widespread deployment of seaweed farms over a substantial fraction of the global oceans, as we expect this would come with unacceptable trade-offs to ocean health[32,45,46], but rather to assess the geographic distribution and potential of offshore seaweed farming to produce harvestable biomass at climate-relevant scales. Our study predicts potential seaweed biomass production in the surface ocean and does not explicitly represent the fate of this biomass after harvest. A companion study[47] uses G-MACMODS to develop a technoeconomic analysis quantifying the costs of seaweed cultivation for carbon removal (e.g., via sinking) or emissions avoidance (e.g., using seaweed for food, animal feed, and biofuels).

Global seaweed harvested yields. Maps in Fig. 1 show the magnitude and types of seaweed harvested in our standard simulations, including the ambient and limited nitrate scenarios; we assume that the seaweed type with the greatest harvested yield is farmed in each grid cell. Results indicate that seaweed could be grown and harvested over large areas of the surface ocean

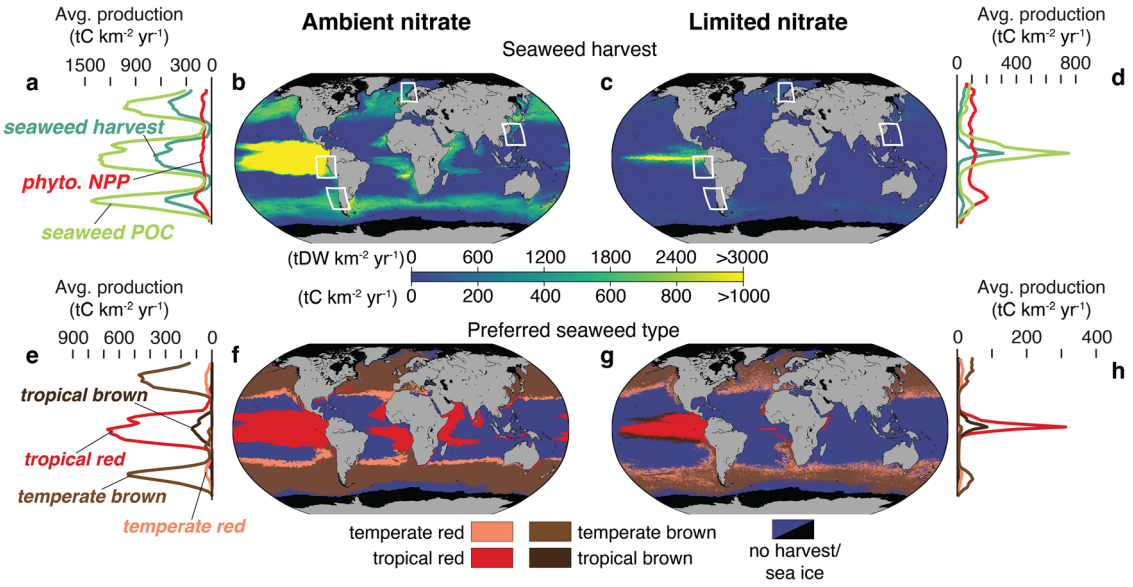

Fig. 1 Global seaweed harvest. Maps of G-MACMODS annual potential harvest per unit area (**b**, **c**) of the preferred seaweed group (the type with the largest harvest in each grid cell; **f**, **g**). While G-MACMODS estimates biomass, we assume that carbon constitutes 30% of seaweed dry weight. White boxes correspond to regions depicted in Fig. 2. Zonally-averaged annual harvest for the preferred seaweed group, seaweed production of particulate organic carbon (POC) and phytoplankton net primary productivity (NPP) estimated from satellite observations[48] are shown in (**a**, **d**). Zonally-averaged annual harvests for the four seaweed types are shown in (**e**, **h**).

(~200 million km^2 and ~130 million km^2 in the ambient and limited nitrate runs, respectively, larger than previous estimates[16,32]); however, annual harvests vary substantially in space and are vastly different between the two nitrate scenarios. The most productive locations include the equatorial Pacific and upwelling regions (e.g., along coasts or near energetic western-boundary currents). Nitrate limitation precludes substantial productivity in oligotrophic regions; thus, almost no seaweed is harvested within the subtropical gyres (Fig. 1b, c).

To provide context for the seaweed harvest distributions simulated by G-MACMODS, we compare seaweed production of particulate organic carbon (POC) to phytoplankton net primary productivity (NPP) estimated from satellite ocean-color observations[48] (Fig. 1a, d). Notably, a substantial fraction of phytoplankton NPP is fueled by nitrate recycled in the euphotic zone; it represents an upper bound on a new product or, similarly, net community production (NCP; typically, NCP < phytoplankton NPP[49]) in the unperturbed natural system. In steady-state, the upper ocean nutrient inventory is set by a balance between biologically-mediated export (e.g., sinking particulate organic matter), equivalent to NCP, and physically-mediated supply; nutrient supply thus comprises an ultimate constraint on the magnitude of NCP.

Macroalgal growth and carbon fixation generally occur at slower rates than in unicellular phytoplankton because the multicellularity and specialized tissues in macroalgae require greater resources[50–52]. However, these specialized structural tissues, including holdfasts and thalli, allow macroalgae to gain access to more persistent light and nutrients at the ocean surface in coastal areas. Moreover, resource storage and mobilization, as well as chemical grazing defenses, permit survival during resource gaps[53,54]. Combined with higher carbon-to-nitrogen (C:N) ratios than phytoplankton[55], these features allow macroalgae to achieve equivalent or greater productivity[56,57], and much greater biomass density[58], than phytoplankton for a given amount of nutrients.

Assuming that nutrient availability is the only constraint to macroalgal growth (neglecting all other growth and nutrient uptake limitations), we expect macroalgal productivity to be proportional to NCP or, as an upper bound on new production, phytoplankton NPP. Seaweed C:N average ~20:1[59,60] to ~40:1[61–63]. These values are ~3–6 times higher than the ~6.6:1 (Redfield ratio) typical of phytoplankton. If seaweed consumed all the nitrogen available to phytoplankton, then we would expect to see, at most, six times as much seaweed POC as phytoplankton NPP. However, in our ambient nitrate simulations, seaweed POC is 10 to 12 times larger than observed phytoplankton NPP, indicating that the modeled seaweed growth under the assumption of nitrate availability surpasses the constraints imposed by nitrate supply (Fig. 1a). This suggests that the ambient nitrate case greatly overestimates the potential productivity of widespread, intensive farming in the absence of artificial upwelling, but it might provide a reasonable estimate of the localized potential harvests of farming operations small enough in scale (e.g., <25 ha[39–41]) so as to not dramatically alter local nitrate budgets. Indeed, the harvested yields simulated in the ambient nitrate scenario agree well with harvest values reported in the literature for many small farms and a few large farms situated near river mouths where nitrogen is likely more abundant (Supplementary Figs. 5–8). In contrast, zonally-averaged production of particulate carbon by seaweed is less than six times the observed phytoplankton NPP in our limited nitrate simulations (Fig. 1d). The lower harvests estimated in the limited nitrate scenario may, therefore, better reflect production when farming at scales large enough to substantially modify or deplete the surface fixed-nitrate inventory, relying on the influx of new nitrate from below the nutricline (Fig. 1c, d).

The standard simulations of both nitrate scenarios predict that temperate brown and tropical red seaweed out-compete temperate red and tropical brown seaweeds over most of the global ocean (Fig. 1f, g). The zonally-integrated annual harvest of tropical red seaweed is ~4–5 times higher than that for tropical brown seaweed; similarly, the zonally-integrated annual harvest of temperate brown seaweed is ~4–12 times larger than that for the temperate reds (Fig. 1e, h).

At regional scales (e.g., areas enclosed by boxes in Fig. 1b, c), physical processes such as western-boundary currents, coastal

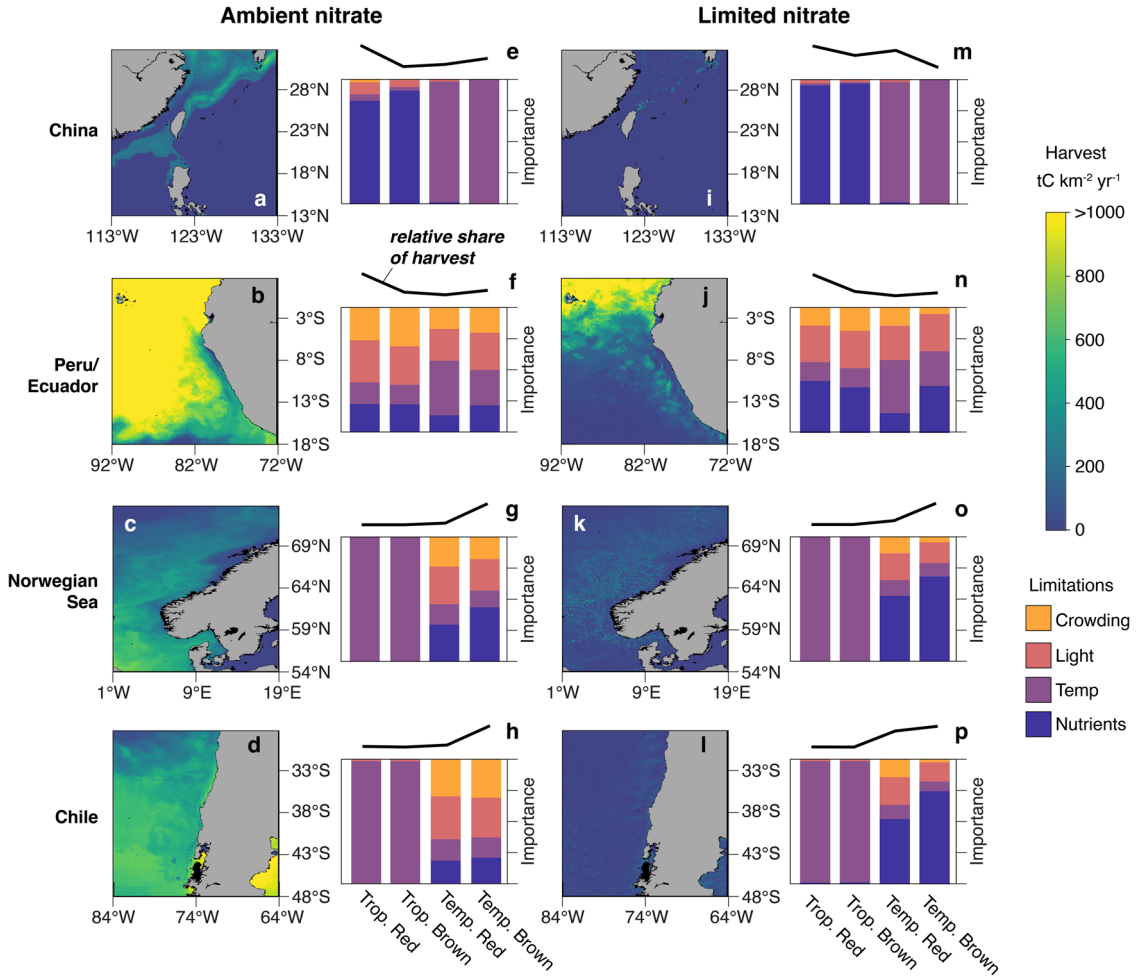

Fig. 2 Regional harvest. (Maps **a**–**d**, **i**–**l**) G-MACMODS annual harvested yields for the boxed regions in Fig. 1, assuming that carbon constitutes 30% of seaweed dry weight. (Bars **e**–**h**, **m**–**p**) The relative influence of growth parameters (equation (7)) in determining regional harvested yield for each seaweed type. (Spark lines) Relative spatially integrated annual harvest for each seaweed type.

upwelling, and frequent eddy activity influence environmental variability and seaweed growth. Within the seaweed growth model, four factors govern seaweed growth rate: water temperature, nitrate availability, light, seaweed density, or crowding (equation (8)). Of these factors, water temperature largely determines the latitudinal distribution of different seaweed types (e.g., tropical seaweeds in the South/East China Sea (Fig. 2, top row) and temperate seaweed in the Norwegian Sea (Fig. 2, third row)). At smaller scales, nitrate availability controls regional patterns of seaweed harvested yield and, as expected, is more important in simulations with limited nitrate than in the ambient nitrate scenario (Fig. 2). Light availability and crowding (e.g., self-shading and sub-grid scale nitrate competition) can become relatively important growth limitation factors in regions with readily available nitrate.

Uncertainty analysis. To assess the sensitivity of our results to uncertainty in the biophysical parameters in G-MACMODS, we conducted a Monte Carlo analysis over a range of literature-based parameter values with uniform distributions (Supplementary Table 1). The standard deviation of Monte Carlo simulations increases in direct proportion to the simulated harvested yield (Fig. 3). For example, regions with larger harvests in our standard simulations also show greater uncertainty in the Monte Carlo results (Fig. 3e, f; Fig. 3a, b as compared to maps in Fig. 1b, c). In the limited nitrate scenario, the average harvested yield in the most productive 10% of the ocean can range from 136–875 tC km^{-2} $year^{-1}$, depending on the values of the biophysical model parameters.

Based on a random forest analysis of Monte Carlo results, the biological parameters that consistently govern the harvested seaweed yield in both nitrate scenarios are the constant mortality rate (not due to waves) and the wave factor (specifically associated with wave mortality), as seen in Fig. 3g, h. Our Monte Carlo simulations evaluate constant mortality rates from 0.003 day^{-1} –0.017 day^{-1}; some prior models have used similar or slightly lower values (0.001 day^{-1} –0.01 day^{-1})[29,30,64,65]. Analogously, the wave factor varies from 0.3 to 1.7, decreasing or increasing the impact of the wave mortality relationship (equation (12)) to address the uncertainties around the wave-driven loss of macroalgal biomass.

The maximum growth rate substantially influences harvest yield in low-productive areas, such as those where less than 250 tC km^{-2} $year^{-1}$ can be harvested (40% and 93% of grid cells in the ambient and limited nitrate simulations, respectively; Fig. 3c, d). Since seaweed is only harvested once it reaches a target weight (see Methods), the maximum growth rate determines whether and how quickly the seaweed reaches a harvestable condition.

Scaling production in EEZs. The maps in Fig. 4 show the area of exclusive economic zones (EEZs) that would be required to harvest seaweed biomass of 1, 2, and 3 GtC $year^{-1}$ in our

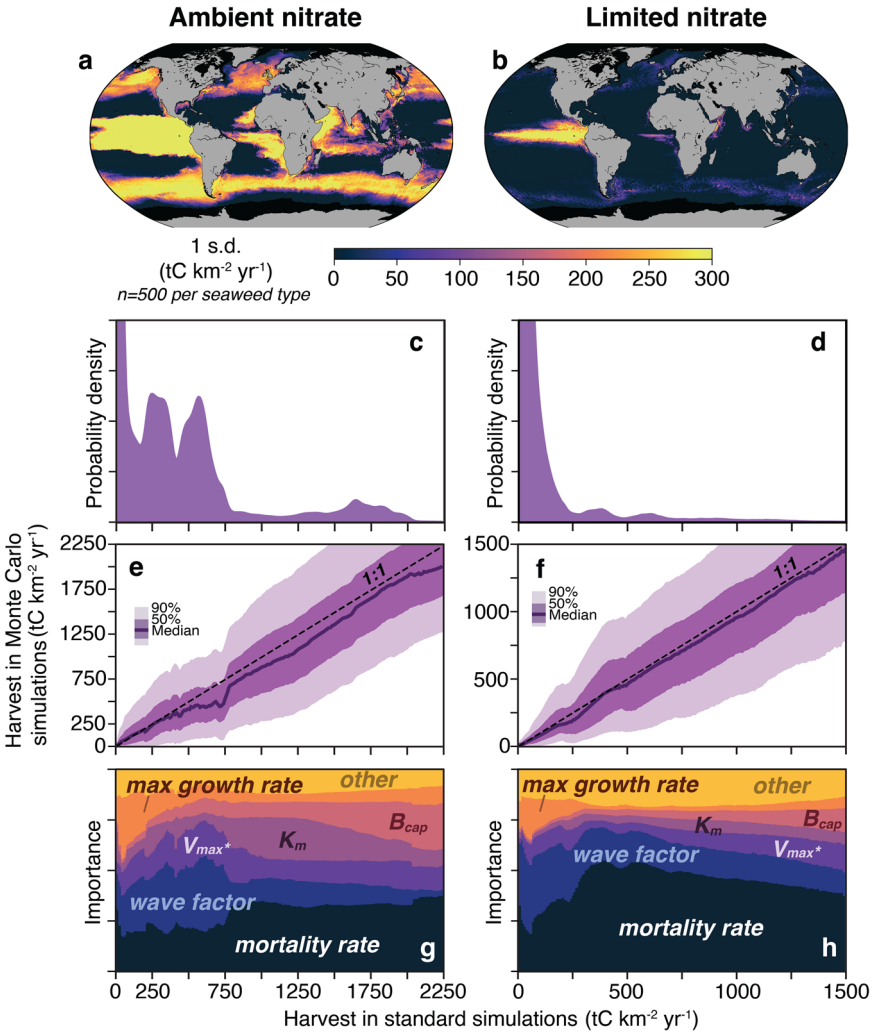

Fig. 3 Harvest uncertainty. Maps of standard deviation from the Monte Carlo results (**a**, **b**) and probability density function (PDF) of the standard run annual harvested yield (**c**, **d**), assuming that carbon constitutes 30% of seaweed dry weight. The y-axis has been cut off to better visualize the smaller PDF values (corresponding to larger harvests). Bin averages of Monte Carlo statistics are shown as a function of the standard run results (**e**, **f**). The median harvest is shown as a solid line; the dark and light shading denotes the values between the 25th and 75th percentiles and the 5th and 95th percentiles, respectively. The dashed 1:1 line shows where the median harvest would lie if it equaled the standard harvest. The relative importance of the biological parameters in Supplementary Table 1, as quantified by random forest analysis, are depicted in (**g**, **h**). V^*_{max} [μmol-N m^{-2} h^{-1}] is the product of the maximum uptake rate (V_{max}) and the ratio of the biomass-to-surface area (B:SA). The biological parameters not explicitly named are grouped under the "other" category (Supplementary Fig. 9).

standard, limited nitrate simulation, assuming that seaweed carbon content is 30% of its dry weight. Figure 4b–d provides examples of productive regions, highlighting local variability. Cumulative distribution functions of annual harvest derived from the limited nitrate simulations as a function of EEZ area (sorted by harvested yield, such that the areas with the largest harvests are cultivated first; Fig. 4e) show diminishing returns from farming more than ~15% of EEZs (locations scattered across the world), with harvests approaching a limit of ~3.5 GtC $year^{-1}$ at ~25% of EEZs (Fig. 4e). In the standard, limited nitrate simulation, the most productive ~0.8% of EEZs (1 million km^2; located in the equatorial Pacific; Fig. 4a, c) is enough to harvest 1 GtC $year^{-1}$, with a range of 0.35 to 1.6 GtC $year^{-1}$ at the 5th to 95th percentiles of the Monte Carlo simulations– less than half the 2.2 GtC $year^{-1}$ harvested in the standard, ambient nitrate simulation (Fig. 4f). Assuming that macroalgal carbon content could constitute as low as 20% or as high as 40% of its dry weight[35], then the area required to harvest 1 GtC $year^{-1}$ would be ~2 million km^2 or 0.8 million km^2, respectively, with corresponding uncertainties of 0.3–1.8 GtC $year^{-1}$ and 0.4–1.6 GtC $year^{-1}$ at the 5th and 95th percentiles.

Discussion and conclusion

This work is an improvement over previous estimates of seaweed productivity and harvestable biomass because it employs a dynamic growth model (G-MACMODS) to simulate seaweed cultivation under two bounding nutrient scenarios and evaluates parametric sensitivities. While excluding some ecosystem feedback, these simulations represent optimistic upper bounds on seaweed production and harvest based on observed biological rates, current farming practices, and ocean physics. The standard simulation model results have been evaluated in comparison to available and relevant published values of farmed and wild seaweed harvested yield (Supplementary Figs. 5–8 and Supplementary Tables 2–5). The ambient nitrate scenario, which assumes that nitrate concentrations are unaffected by seaweed farms, represents a global extrapolation of non-intensive seaweed

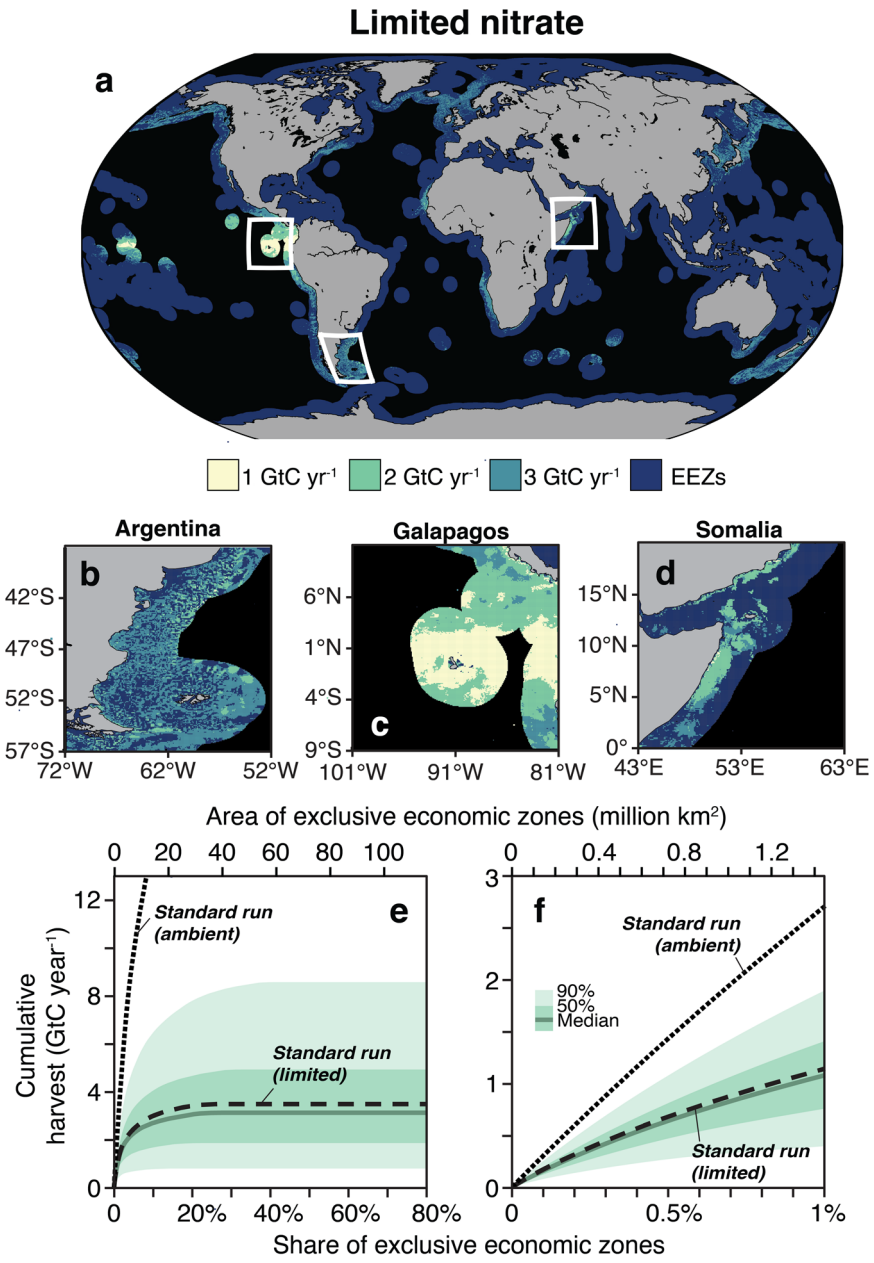

Fig. 4 Total potential harvest in EEZs. a–d Areas of exclusive economic zones (EEZs) required to harvest 1, 2, and 3 GtC year^{-1} of seaweed biomass in standard, limited nitrate simulations, sorted by harvested yield (i.e., prioritizing the most productive areas). The white boxes in (**a**) correspond to the locations depicted in (**b**–**d**). **e**, **f** Cumulative distribution functions of total seaweed carbon harvested relative to the share of global EEZs farmed. Results from the ambient and limited nitrate standard runs are depicted as dashed lines. The solid green line and surrounding shading indicate the range of harvests of Monte Carlo, limited nitrate simulations. While G-MACMODS estimates biomass, we assume that carbon constitutes 30% of seaweed dry weight.

farming, similar to many current efforts in coastal areas[39–41]. However, under high-density, intensive farming it is clear that depleted nitrate could not be replaced through transport from the surrounding environment without quickly straining the inventory of near-surface ocean nutrients and disrupting the natural biological carbon pump[32]. Sustaining the levels of production simulated in the ambient nitrate scenario over large areas would thus require some form of nitrate amendments (e.g., artificial upwelling or depth-cycling[23]) which would, in turn, entail additional costs and environmental consequences. Our limited nitrate simulations reflect optimistic upper bounds of offshore seaweed production that might be supported by using only the new nitrogen that is naturally replenished from the deep ocean (fluxed upward across the 100-m depth plane through natural upwelling and mixing processes and not artificially upwelled). Relative to the ambient scenario, the limited nitrate simulations reduce potential seaweed harvest worldwide by a median of 90%.

Recent studies on macroalgae farming highlight this industry's potential to offset greenhouse gas emissions[5,15–17] without addressing geographical variability in seaweed productivity. In this study, using the limited nitrate simulations, we estimate that a climate-relevant mass of carbon (e.g., 1 GtC year^{-1}) could be harvested by farming seaweed in the most productive 0.8% of EEZs worldwide (Fig. 4f; ~1 million km^2), representing a ~370-fold increase in the area where seaweed is currently farmed (~2500 km^2 [66,67]). For comparison, the area occupied by all

agricultural cropland in the United States is ~1.6 million km^2 [68]. The US National Academy of Sciences, Engineering, and Medicine suggests that, as one of several CDR strategies, seaweed cultivation could play a meaningful role in atmospheric CO_2 reduction at an extraction level of ~0.03 GtC year^{-1}[15]; however, even this target requires increasing the current seaweed cultivation area by over tenfold, sustaining high yields in the most productive regions of the ocean, and ensuring that harvested biomass is sequestered. Reaching climate-relevant carbon targets is even more challenging when cultivating seaweed outside of the most productive areas of the EEZs (the equatorial Pacific). Harvesting 0.1–1 GtC year^{-1} outside of the most productive 1 or 5% of the EEZs, would require growing macroalgae over 200,000–3 million km^2 or 1 million–24 million km^2, respectively, according to our standard runs. This is similar in magnitude to existing estimates[15,69] yet beyond the capacity of the current seaweed-farming industry. When entertaining such massive changes to the ocean for offsetting greenhouse gas emissions, we must also consider technoeconomic challenges[47], as well as limits to CO_2 removal due to time scales of air-sea carbon fluxes, and disruptions to the natural biological carbon pump[32,70,71].

As indicated by the spread across the Monte Carlo simulations, the largest uncertainties in our estimates of seaweed harvest correspond to biophysical parameters related to seaweed mortality, which we divide into a wave-related erosion term, and a constant loss term, set at 1% per day, that accounts for senescence, dislodgement, disease, epiphytic infestation, grazing, and other loss processes. The wave-loss term (d_w, equations (12, 13)) varies with significant wave height (H_s) and wave period (T_w). As an example of its magnitude, for $H_s = 1$ m and $T_w = 12$ s, the wave-loss term would reach $d_w = 0.3\%$ per day. Existing models and observations span both lower[29,30,32,65,72] and higher mortality rates[59,73,74], yet these sources, which primarily consider nearshore farms, often do not distinguish between wave-related mortality and other sources of loss, and may have limited applicability to mortality on open ocean farms. Moreover, real mortality might be episodic and associated with disturbance events like storms or disease outbreaks. Our results thus highlight the importance of further research to constrain seaweed mortality under the conditions faced during cultivation to improve harvest predictions.

Using the dynamic biophysical seaweed growth model, G-MACMODS, we estimate the global potential for seaweed farming in detail. Our results suggest that biophysical ocean limits may support annually harvested seaweed containing 1 GtC year^{-1} from intensive farming in ~1 million km^2 of the most productive ocean areas. However, practical, but different assumptions about the geographical location of farms, farming intensity, and the optimization of seeding and harvesting can cause the estimates of the area required to reach the same 1 GtC year^{-1} goal to increase substantially. In addition to narrowing uncertainties and accounting for the effects of climate change, future work must further assess the economic and political feasibility of farming seaweed over large areas that may have other uses or protections (e.g., fishing, shipping traffic, and marine protected areas). Similarly, if the purpose of harvesting such large quantities of seaweed is to sink it into the deep ocean and thereby sequester carbon, the effects on abyssal ecosystems[75–77] and the possibility of increasing the extent of hypoxic regions[78,79] deserve more investigation[80]. Given that there remain many unknowns and hurdles for large-scale seaweed farming, our analysis suggests that refinement of the global seaweed cultivation potential warrants investment in future research.

Methods

G-MACMODS overview. The Global MacroAlgae Cultivation MODeling System (G-MACMODS) used in this study draws on recent work on within-farm biophysics[33], using elements from previously published research[27–29]. The state variables in the model are seaweed biomass (B; g-DW m^{-2}; where DW is dry weight) and nitrogen cell quota (Q; mg-N g-DW^{-1}[81]). Nitrogen in the form of nitrate is the limiting macronutrient in G-MACMODS, although other forms of nitrogen (e.g., ammonium and urea) can contribute to seaweed growth in low-nitrate environments[37,38]. We recognize that other macronutrients and micronutrients could further limit our results in, for example, high-nitrogen, low chlorophyll environments[82]. G-MACMODS estimates seaweed biomass in units of dry weight; biomass is converted to units of carbon by assuming that carbon constitutes 30% of the seaweed dry weight for all seaweed groups[35,83,84], though carbon content may vary across time, space, and genus[35,62]. We address how other carbon-content assumptions affect our conclusions under the section Scaling Production in the EEZs.

A diagram of the conceptual model is presented in Supplementary Fig. 1. The model has a daily time step and considers macroalgae to be grown at 2 m depth below the surface for the purposes of light attenuation. Seaweed biomass is depth-integrated across the top 20 m of the water column to account for the depth of kelp cultivation.

G-MACMODS state variables. Temporal changes in the state variables (B and Q) can be described with the following equations:

$$dQ = Vdt + Q\left(\frac{1}{1+\mu dt} - 1\right) - E(Q - Q_{\min})dt, \quad (1)$$

and

$$dB = \mu B dt - d_M B dt, \quad (2)$$

where V is the nitrogen uptake rate [μmol-N (g-DW h)$^{-1}$], E is a fractional exudation rate (day^{-1}; Supplementary Table 1), μ is the fractional growth rate (day^{-1}; equation (7)), and d_M is the total fractional death rate (day^{-1}; equation (12)).

G-MACMODS nitrogen uptake. The rate of nitrogen uptake by seaweed is determined by extrinsic (environmental) and intrinsic (biological) limiting factors:

$$V = V_{\max} f(Q) f(|\mathbf{u}|, T_w, C), \quad (3)$$

where $V_{\max}$ is the maximum uptake rate (Supplementary Table 1), $f(Q)$ represents a dynamic nitrogen cell quota which allows for luxury uptake of nitrogen, and $f(|\mathbf{u}|, T_w, C)$ represents both kinetic and mass-transfer limitations on nitrogen uptake. We use a linear nitrogen cell quota[33]:

$$f(Q) = \frac{Q_{\max} - Q}{Q_{\max} - Q_{\min}}, \quad (4)$$

where $Q_{\min}$ is the minimum amount of nitrogen that should be found in a seaweed cell (structural nitrogen), $Q_{\max}$ is the maximum amount of nitrogen stored internally, such that uptake decreases as the internal nitrogen concentration increases, and $f(Q)$ is a unitless coefficient between 0 and 1. The parameter $f(|\mathbf{u}|, T_w, C)$ in equation (3) is a limit on uptake based on a combination of Michaelis–Menten kinetics and mass-transfer limitation regulated by the surrounding waves and currents[85–87] :

$$f(|\mathbf{u}|, T_w, C) = \frac{C}{K_m\left(\frac{C}{K_m} + \frac{1}{2}\left(\gamma + \sqrt{\gamma^2 + 4\frac{C}{K_m}}\right)\right)}, \quad (5)$$

where $\gamma = 1 + (V_{\max}/\beta K_m) - (C/K_m)$, K_m is the half-saturation constant (Supplementary Table 1), C is the external concentration of nitrogen, and

$$\beta = \frac{D}{\delta_D} + \frac{4\delta_D}{T_w}\sum_{n=1}^{\infty}\left(\frac{1 - \exp\left(\frac{-Dn^2\pi^2 T_w}{2\delta_D^2}\right)}{n^2\pi^2}\right) \quad (6)$$

with units of m s^{-1}. In equation (6), D is the molecular diffusivity of nitrate at 18° C (7.3×10^{-10} m^2 s^{-1})[33,88], T_w is wave period, and δ_D is the thickness of the diffusive boundary layer, defined using the thickness of the viscous boundary layer $\delta_D = \delta_\nu = 10\nu/(\sqrt{C_D}|\mathbf{u}|)$ where ν is the molecular kinematic viscosity (10^{-6} m^2 s^{-1}) and C_D is the drag coefficient[87] (Supplementary Table 1). The parameter $f(|\mathbf{u}|, T_w, C)$ is unitless and varies between 0 and 1. Note that this nitrogen uptake model assumes that (a) the diffusive boundary layer is completely stripped away every half a wave period, regardless of the size of the wave, (b) the thickness of the diffusive boundary layer (δ_D) can be parameterized with the thickness of the viscous boundary layer (δ_ν), and (c) that we can ignore near-boundary turbulent transport (i.e., assume the blade is smooth)[87], though this has been shown to enhance exchange rates[89]. We do not consider within-canopy flow reduction, which negatively affects uptake[33,90]. We assume that wave height has a negligible effect on uptake, since renewal of the diffusive boundary layer (and, hence, enhanced nitrate uptake) can occur through blade flapping in a low-flow environment[91]. Thus, equation (3) is used to estimate the amount of nitrogen that the seaweed could, theoretically, take up from the environment (dN).

Two nitrate scenarios are tested in this study: (1) a case where nitrate concentrations from a global ocean model (CESM) are averaged over the top 20 m

of each grid cell and are available to seaweed without depletion or competition is referred to as the ambient nitrate scenario and (2) a case where the amount of nitrate available for uptake is capped by the nitrogen that is naturally fluxed upward through the 100-m depth plane (N_{new}), referred to as the limited nitrate scenario. In the limited nitrate scenario, the nitrogen uptake rate (equation (3)) is still determined by the ambient (average of top 20 m) nitrate concentration, but if the amount of nitrogen that would be theoretically taken up by seaweed at a given time is greater than that fluxed upward at 100 m depth, $dN > N_{new}$, then uptake (V in equation (1)) is capped using $dN = N_{new}$. Additional simulations were performed to test an alternate depth for estimating N_{new}—at the annual maximum mixed-layer depth at each grid cell—but resulting harvested yield differences were relatively small compared to other uncertainties presented in the Uncertainty Analysis section (median increase of 6% in the annual harvest).

G-MACMODS growth. Similar to the nitrogen uptake rate, growth rate (μ) is also constrained by extrinsic and intrinsic limiting factors:

$$\mu = \mu_{max}\, g(k)\, g(Q)\, g(T)\, g(E). \tag{7}$$

The maximum growth rate allowed under ideal conditions (μ_{max}) is constrained by crowding effects that account for self-shading and sub-gridscale nutrient limitations [$g(k)$], internal nitrogen reserves [$g(Q)$], water temperature [$g(T)$], and light [$g(E)$], all of which are represented by unitless coefficients, varying between 0 and 1.

The growth rate limitation imposed by crowding in the seaweed canopy [$g(k)$] embodies the general idea that less-dense seaweed can grow faster, or

$$g(k) = \frac{k_R}{\mu_{max}} \left(\frac{B}{B_{cap}}\right)^{-0.75}, \tag{8}$$

where B_{cap} (g-DW m^{-2}) is the biomass density at which seaweed grows by a fraction $k_R = 0.05$ day^{-1} under ideal conditions. We tuned B_{cap} to match field observations from the literature (see Model-Field Data Comparison). The power law in equation (8) was derived by re-fitting data from a comprehensive meta-analysis[92]. Our fit was applied to the data in ref. [92] and binned to 0.01-width bins from 0–1 g L^{-1} and 0.1-width bins for 1–60 g L^{-1} seaweed density, weighted by the number of observations in each bin (with a minimum weight of eight observations). Our fit excluded data corresponding to total-nitrogen ($NO_3 + NH_4$) conditions not likely to be found in the surface ocean (values above 20 μM). Although according to equation (8), $g(k) \to \infty$ as $B \to 0$, we cap $g(k)$ at 1.

The nitrogen quota limitation $g(Q)$ in equation (7) is a modified form of the Droop model[81]:

$$g(Q) = \frac{Q - Q_{min}}{Q} \frac{Q_{max}}{Q_{max} - Q_{min}}. \tag{9}$$

where Q_{min} and Q_{max} are set per seaweed type (Supplementary Table 1). The temperature limitation term in Equation (7) is similar to a Gaussian probability curve[93]:

$$\begin{aligned} g(T) &= \exp(-\beta_1 (T - T_{opt})^2), T < T_{opt} \\ g(T) &= \exp\left(-\beta_2 (T - T_{opt})^2\right), T > T_{opt} \\ g(T) &= 1, T = T_{opt}, \end{aligned} \tag{10}$$

where T_{opt} is a 5° optimal temperature range for each seaweed group (Supplementary Table 6), T is the daily temperature, and the β_1 and β_2 coefficients are adjusted to reach zero near the lower- and upper-temperature limits, respectively.

The light limitation in equation (7) is largely informed by phytoplankton studies[94]:

$$g(E) = f \frac{I - I_c}{I_s - I_c} \exp\left(-\frac{I - I_c}{I_s - I_c} + 1\right), \tag{11}$$

where I_s and I_c are the daily-averaged saturating and compensating irradiance (W m^{-2}), f is the fraction of daylight that is implemented to account for periods of darkness, and I is the irradiance reaching an underwater depth of 2 m. The irradiance is attenuated following the implementation in the Marine Biogeochemistry Library (MARBL)[95,96].

G-MACMODS mortality. The total mortality rate, d_M in equation (2), is the sum of a constant daily mortality rate that is meant to incorporate grazing, aging, and disease (d; Supplementary Table 1) and a term that accounts for breakage from waves (d_w), such that

$$d_M = d + \Pi d_w. \tag{12}$$

The d_w term is dependent on wave power and, as such, is variable in both time and space[97]:

$$d_w = (2.3 \times 10^{-4})(P \times 10^{-3}) + 2.2 \times 10^{-3}, \tag{13}$$

where P is wave power in Watts:

$$P = \frac{\rho g^2}{64\pi} H_s^2 T_w \tag{14}$$

where ρ is the density, H_s is the significant wave height, and T_w is the wave period. Ref. [98] offers a different macroalgal wave mortality equation, but the one we implement penalizes seaweed growth to a lesser degree. However, in equation (12), Π (Supplementary Table 1) is a wave factor that accounts for the uncertainty surrounding the use of a single equation to represent wave mortality across all seaweed types. For our standard runs, $\Pi = 1$ and $d_M = d + d_w$.

Environmental data. The environmental inputs applied to our model (water temperature, solar irradiance, current velocities, wave height, wave period, and nitrate concentrations) stem from a combination of satellite measurements and global ocean model outputs spanning multiple years. For the purposes of this manuscript, we explore a suite of simulations using inputs from 2017, the most recent year with available data that is also not identified as having a strong ENSO index. Input data from 2003–2019 were used in simulations examining interannual differences in estimated seaweed growth (Supplementary Fig. 11); however, regional interannual variability was comparatively small with respect to parameter uncertainty and is therefore not the focus of this study.

Sea surface temperature (SST) and surface photosynthetically active radiation (PAR) are used as a proxy for in situ temperature and irradiance, respectively, over the depth of macroalgal growth. SST and PAR used in this study are 8-day averages from the Moderate Resolution Imaging Spectroradiometer (MODIS; R2018), on the NASA Earth Observing System, with a spatial resolution of 1/12°. Net oceanic primary productivity (NPP) was estimated from MODIS chlorophyll measurements using the Vertically Generalized Production Model (VGPM)[48]. SST, PAR, and NPP were downloaded from the Ocean Productivity website[99,100].

Zonal and meridional current velocities were extracted from the HYbrid-Coordinate Ocean Model (HYCOM[101]) Global Ocean Forecasting System (GOFS) 3.1[102]. HYCOM is a global data-assimilating model[103] with 1/12° horizontal resolution and 41 depth levels, of which we use the surface velocities.

Significant wave height and wave period were taken from the European Centre for Medium-Range Weather Forecasts (ECMWF) ERA5[104] atmospheric reanalysis produced by the Copernicus Climate Change Service[105]. ERA5 provides hourly significant wave height of combined wind waves and swell, and mean wave period with a 1/2° horizontal resolution. The data were averaged in 8-day time intervals.

Nitrate information is taken from a high-resolution biogeochemical simulation led by the National Center for Atmospheric Research (NCAR) and run in the Community Earth System Model (CESM) framework[106–108]. The biogeochemical model has a 1/10th ° horizontal resolution and 62 depth levels. Fields used in this study include 5-day mean nitrate concentrations averaged over the upper 20 m, and vertical fluxes of nitrate across the 100-m depth plane were calculated to provide an estimate of fluxes of new nitrogen into the euphotic zone.

Although G-MACMODS steps forward with a daily time step, we apply the 8-day environmental inputs that best correspond to the G-MACMODS time stamp. All environmental inputs were spatially interpolated onto a 1/12 ° global grid, using linear interpolation if the input data were of higher resolution, or nearest-neighbor if the input data were of lower resolution.

Seaweed groups. Here, we focus on four seaweed groups containing seaweed genera that are among the world's ten most cultivated by weight[109]: tropical reds (e.g., *Eucheuma, Kappaphycus*), tropical browns (e.g., *Sargassum*), temperate reds (e.g., *Pyropia*), and temperate browns (e.g., *Saccharina, Laminaria,* and *Macrocystis*). Values of parameters required by G-MACMODS were gathered from available literature for a few representative seaweed genera (Supplementary Table 1); standard runs were defined using average (when multiple parameter estimates were available) or speculated values (based on information from other genera when there were few or no published values), though we modify some of the values implemented in the standard runs to improve comparison with the field data (see the section on Model-Field Data Comparison). We define the temperature parameters in equation (10) similarly, using available information for representative genera (Supplementary Table 6). The optimal temperature range in equation (10) is extended to a 5° width, rather than a single number, to account for variations within a seaweed genus.

The standard runs were spun up for 1 year, and the seeding was optimized by choosing the run initialization date that yielded the largest yearly biomass harvest (averaged across 2003–2019) for every grid point. Tropical and temperate brown seaweed runs were seeded with 50 g-DW m^{-2}. Tropical and temperate red seaweed runs were seeded with 200 g-DW m^{-2} and 10 g-DW m^{-2}, respectively, following examples in the literature (see Supplementary Tables 2–5). Seaweed are seeded with an initial nitrogen cell quota (Q_0), such that

$$Q_0 = Q_{min} + \frac{N}{35}(Q_{max} - Q_{min}), \tag{15}$$

where N/35 is the ratio of the ambient nitrogen concentration at the time of seeding to the a representative N concentration below the nutricline (35 μM).

Model-field data comparison. To test our choice of standard parameters (Supplementary Table 1) and calibrate B_{cap} (equation (8)), we compared biomass from our G-MACMODS standard runs to published observations of seaweed mariculture and wild seaweed standing stock surveys. Only farmed values published after the year 2000 are included in this comparison to account for changes in technology and methods across the years, whereas we include wild stock values from literature published as far back as 1990. Overall, G-MACMODS produces a range of biomass that agrees with what has been observed in published field studies (Supplementary Figs. 5–8). We carried out further detailed comparisons to examine the performance of G-MACMODS at the locations specified in the published studies. To do so, we applied the following protocols to our analysis:

- If the published manuscript mentioned specific coordinates or a coordinate range, we found the spatial mean of our variable of interest within a 50 km radius of the specified coordinates or within the specified coordinate range, respectively. If the manuscript included a map with sampling locations (no specific coordinates) or enough geographic information to narrow down a location to a single point, we found the most representative coordinates of that location and calculated the spatial mean of our variable of interest within a 50 km radius of those representative coordinates. However, if the manuscript did not provide enough information to narrow down a location to a specific point, then we estimated the spatial mean of our variable of interest within a 3° × 3° box in the general region of the published study.
- If the published manuscript reported biomass, rather than harvest weight, we compared the article's maximum attained biomass to the maximum biomass grown in G-MACMODS over the course of the specified harvest cycle at the corresponding location.
- Any biomass reported in fresh weight is converted to dry weight using a 10:1 ratio.
- Unless otherwise specified, these G-MACMODS simulations use the 2017 temperature, PAR, current velocity, and wave fields typical of our standard runs.

We applied some additional protocols that vary across seaweed types:

1. Tropical red seaweed: The G-MACMODS simulations were seeded with a biomass density equivalent to that used in the referenced publications; the biomass was harvested back to seed weight at the corresponding harvest period (Supplementary Table 2). If the referenced publications did not provide seed or harvest period information, then we assumed a seed density of 200 g-DW m^{-2} and a 45-day harvest period, which was the most common farming configuration. The validations were run with a constant nitrate concentration comparable to the maximum nitrate concentration reported for each field experiment; if no nitrate information was available, we used the CESM nitrate field previously described under the Environmental Data subsection of the Methods. We compared the temporal maximum of the G-MACMODS harvested biomass to the mean harvest yield reported in the corresponding literature to examine whether G-MACMODS could approximate the values observed in the field, notwithstanding the lack of information from the published field studies. The G-MACMODS runs for these comparisons did not include wave energy, since most tropical red seaweed cultivation takes place in shallow sheltered areas.
2. Tropical brown seaweed: Given that the published studies that we reference report wild seaweed standing stock (Supplementary Table 3), we did not include harvesting in the G-MACMODS comparison simulations. The seeding process, however, followed the protocol established for our standard runs. In addition, these G-MACMODS simulations did not include wave energy and used the CESM nitrate field previously described under the Environmental Data subsection of the Methods.
3. Temperate red seaweed: We simulated temperate red macroalgae cultivation across the same time period as specified in the published literature (Supplementary Table 4) using an identical harvest scheme and seed density to that applied in our standard runs. When reported, we applied the mean NO_3 concentration in the field studies to the G-MACMODS simulations. As a metric of model performance, we compared the harvest yield from the G-MACMODS simulations to the mean harvested biomass from the literature.
4. Temperate brown seaweed: We simulated temperate brown seaweed cultivation across the same time period as specified in the published literature (Supplementary Table 5), assuming a biomass density of 50 g-DW m^{-2} after 30 days of cultivation, with only one harvest at the end of the cultivation period, when applicable. We did not include harvesting in the G-MACMODS simulations that try to reproduce field studies of macroalgal standing stock. If reported, we applied the mean NO_3 concentration in the field studies to the G-MACMODS simulations. When relevant, we compared the harvest yield from the G-MACMODS simulations to the mean harvested biomass from the literature using units of g-DW m^{-1}, assuming a 1-m line separation in the G-MACMODS simulations. Waves were included in these G-MACMODS simulations.

Overall, G-MACMODS has the capacity to produce biomass at the levels observed in published field studies (Supplementary Figs. 5–8, panel b). Some of the more specific comparisons do not agree with each other (Supplementary Figs. 5–8, panel c); however, we expected some disagreement since, in many cases, we lacked the information to adequately reproduce individual studies' field conditions. For example, many studies did not include any nitrate information (Supplementary Tables 2–5). While the CESM nitrate fields were, at times, enough to replicate the conditions in the published studies, the CESM NO_3 cannot account for farming practices that include nitrate fertilization[110] or the placement of seaweed farms downstream of a substantial nitrate source (e.g., fish farm, river outlet, or other coastal feature). Given those exceptions, we find G-MACMODS to perform adequately when compared to field data.

Harvest. Harvest schemes were based on available information of current farming practices[20,32,39–41,111,112] and optimized for each seaweed group to achieve maximal biomass per harvest based on standard run tests of three harvest schemes: periodic harvesting, periodic harvesting with a biomass threshold, and conditional harvesting (with dual criteria of a target weight or when death exceeds growth). The test runs also allowed for optimization of the target weight to initiate harvest (10, 20, 30, 40, 50, or 80% of B_{cap}), as well as the percent of biomass removed at each harvest (40, 60, or 80%). Finally, the number of harvests per year were limited based on documented cultivation practices. The temperate brown and red algae are commonly harvested twice[20] and six times a year[111], respectively, while the tropical brown and red algae are harvested up to eight times a year[40,113]. Temperate brown seaweeds were allowed to grow without consideration for harvest for at least 60 days after seeding. Considering the above factors, the harvesting schemes that produced the highest harvested yields for each seaweed group are as follows:

1. Tropical red and brown seaweeds: Harvest occurs every 45 days only if the seaweed biomass has reached the target weight of 800 g-DW m^{-2} (40% of B_{cap}) for tropical reds and 400 g-DW m^{-2} (80% of B_{cap}) for tropical browns. If 45 days elapse and the seaweed does not reach its target weight, another 45-day period must transpire before re-evaluating the biomass. If the biomass has reached its target weight, then 80% of the biomass is harvested.
2. Temperate red seaweeds: Harvest is initiated whenever the biomass reaches the target weight (80 g-DW m^{-2}, 64% of the B_{cap}) within 150 days after seeding or if the death exceeds growth for 7 days. If the biomass has reached its target weight, then it is harvested down to 60 g-DW m^{-2}. If the death exceeds growth for >7 days or the final harvest period is reached, 99% of the biomass is harvested (1% loss rate assumed in the final total harvest).
3. Temperate brown seaweeds: Harvest occurs when the biomass reaches the target weight (1350 g-DW m^{-2}, 68% of the B_{cap}) within 220 days after seeding or if death exceeds growth for 7 days. If the biomass has reached its target weight, then 80% of the biomass is harvested; if the death exceeds growth for >7 days or the end of 220 days is reached, 99% of the biomass is harvested (1 % loss rate assumed in final total harvest).

Monte Carlo simulations. We used Monte Carlo methods to estimate the uncertainty surrounding our standard run harvest amounts. We performed between 497–534 Monte Carlo simulations for each seaweed group and nutrient scenario (ambient vs. limited nitrate). Each Monte Carlo simulation chose the value of the seaweed biological parameters using a uniform probability distribution bounded by the magnitudes in Supplementary Table 1. When possible, these bounds are 25% greater (lower) than the maximum (minimum) biological parameter values found in the literature. However, we prioritized having symmetric bounds over bounds that cover the range of values in the literature to aid the interpretation of the results. The mean, median, standard deviation, and percentiles (5th, 25th, 75th, and 95th) of annual harvested yields resulting from these Monte Carlo simulations were calculated across each model grid cell. The relative importance of each Monte Carlo parameter value upon harvested biomass was evaluated using random forest analysis.

Model limitations. G-MACMODS and our scenarios are subject to a number of important limitations and caveats. First, operating farms will not have the benefit of hindsight that our model uses to optimize seeding and harvest schedules, and the model assumptions are optimistic with regard to micronutrient fertilization and environment/strain optimization in cultivars. Second, neither of the implemented nutrient scenarios considers how seaweed farms affect the surrounding hydrodynamics, which can substantially affect nitrate uptake and yields[33] but are challenging to resolve in a global-scale model. We expect that densely-packed farms would impede thinning of the diffusive boundary layer, thus reducing macroalgae's ability to take up nitrate. Third, the nitrate data (from CESM simulations) do not resolve nitrate runoff in coastal areas[114], sources of nitrogen other than nitrate (e.g., ammonium or urea), nor consider other limiting macronutrients such as phosphate. However, standard ambient nitrate runs using a second set of nitrate inputs from a biogeochemical hindcast model that incorporates riverine nutrients (produced at Mercator-Ocean and distributed by E.U. Copernicus Marine Service Information; DOI:10.48670/moi-00019) suggests that the uncertainty associated with the source of nutrients is within the range of uncertainty related to the biological parameters in our model (Supplementary Fig. 10).

G-MACMODS would also benefit from a more refined expression of seaweed mortality that could account for episodic events (e.g., storms, diseases) and nonlinear grazing pressure, among other factors, as well as an improved understanding of wave mortality for different genera. Moreover, we do not explicitly model the effects of climate change and projected changes in ocean conditions that can stress growing seaweeds, shift their geographical distribution, increase the frequency and severity of storms, decrease nitrate fluxes by enhanced stratification, and make diseases and epiphytes more prevalent[115,116]. These are important areas for future research. Although certainly not a proxy for the many effects of climate change, we note that interannual variability in environmental forcing (2003–2019) affects our harvest estimates less than the uncertainties related to biological parameters (Supplementary Fig. 11).

Data availability

To facilitate reproducibility and enable further analysis, we provide access to the G-MACMODS output presented in the main manuscript and the Supplementary Information through https://doi.org/10.7280/D1VT4V. The G-MACMODS simulations admit a variety of environmental inputs, as described in Methods. For the simulation results presented in this manuscript, we used MODIS sea surface temperature (SST), MODIS surface photosynthetically active radiation (PAR), and net oceanic primary productivity (NPP) downloaded from the Ocean Productivity website (https://sites.science.oregonstate.edu/ocean.productivity/index.php). Specifically, 8-day NPP can be found at http://orca.science.oregonstate.edu/1080.by.2160.8day.hdf.vgpm.m.chl.m.sst.php, whereas 8-day MODIS inputs are from https://sites.science.oregonstate.edu/ocean.productivity/1080.by.2160.8day.inputData.php. Zonal and meridional surface current velocities were taken from the HYbrid-Coordinate Ocean Model (HYCOM99) Global Ocean Forecasting System (GOFS) 3.1, accessed from https://www.hycom.org/dataserver/gofs-3pt1/analysis. Significant wave height and wave period were taken from the European Centre for Medium-Range Weather Forecasts (ECMWF) ERA5 atmospheric reanalysis (DOI: 10.24381/cds.adbb2d4). Surface nitrate concentrations and vertical nitrate fluxes can be found in the UCAR/NCAR - GDEX (https://doi.org/10.5065/hpae-3j62).

Code availability

The code and documentation for G-MACMODS are now accessible to the public via GitHub (https://github.com/macmods/G-MACMODS.git).

Received: 7 September 2022; Accepted: 2 May 2023;
Published online: 15 June 2023

References

1. DeAngelo, J. et al. Energy systems in scenarios at net-zero CO_2 emissions. *Nat. Commun.* **12**, 1–10 (2021).
2. IPCC. Summary for policymakers. *Climate Change 2021: The Physical Science Basis. Contribution of Working Group I to the Sixth Assessment Report of the Intergovernmental Panel on Climate Change* (2021).
3. Vijn, S. et al. Key considerations for the use of seaweed to reduce enteric methane emissions from cattle. *Front. Vet. Sci.* **7**, 1135 (2020).
4. Roque, B. M. et al. Red seaweed (*Asparagopsis taxiformis*) supplementation reduces enteric methane by over 80 percent in beef steers. *PLOS ONE* **16**, e0247820 (2021).
5. Spillias, S. et al. Reducing global land-use pressures with seaweed farming. *Nat. Sustain.* **6**, 1–11 (2023).
6. Milledge, J. J., Smith, B., Dyer, P. W. & Harvey, P. Macroalgae-derived biofuel: A review of methods of energy extraction from seaweed biomass. *Energies* **7**, 7194–7222 (2014).
7. Michalak, I. Experimental processing of seaweeds for biofuels. *Wiley Interdiscip. Rev. Energy Environ.* **7**, e288 (2018).
8. Ravanal, M. C. et al. Production of bioethanol from brown algae. In *Advances in Feedstock Conversion Technologies for Alternative Fuels and Bioproducts* (ed. Hosseini, M.) Ch. 4 (Elsevier, 2019).
9. Liu, J. J. et al. Production of fuels and chemicals from macroalgal biomass: Current status, potentials, challenges, and prospects. *Renew. Sustain. Energy Rev.* **169**, 112954 (2022).
10. Bhuyan, M. et al. Seaweed: A Powerful Tool for Climate Change Mitigation That Provides Various Ecological Services. *Bangladesh II: Climate Change Impacts, Mitigation and Adaptation in Developing Countries* (ed. Dodson, J.) Ch. 5 (Springer, 2021).
11. He, P. et al. Bioremediation efficiency in the removal of dissolved inorganic nutrients by the red seaweed, *Porphyra yezoensis*, cultivated in the open sea. *Water Res.* **42**, 1281–1289 (2008).
12. Huo, Y. Z. et al. Bioremediation efficiencies of *Gracilaria verrucosa* cultivated in an enclosed sea area of Hangzhou Bay, China. *J. Appl. Phycol.* **23**, 173–182 (2011).
13. Xiao, X. et al. Nutrient removal from Chinese coastal waters by large-scale seaweed aquaculture. *Sci. Rep.* **7**, 1–6 (2017).
14. Jiang, Z. et al. Kelp cultivation effectively improves water quality and regulates phytoplankton community in a turbid, highly eutrophic bay. *Sci. Total Environ.* **707**, 135561 (2020).
15. National Academies of Sciences, Engineering, and Medicine. *A Research Strategy for Ocean-based Carbon Dioxide Removal and Sequestration* (The National Academies Press, 2021).
16. Froehlich, H. E., Afflerbach, J. C., Frazier, M. & Halpern, B. S. Blue growth potential to mitigate climate change through seaweed offsetting. *Curr. Biol.* **29**, 3087–3093 (2019).
17. Duarte, C. M., Bruhn, A. & Krause-Jensen, D. A seaweed aquaculture imperative to meet global sustainability targets. *Nat. Sustain.* **5**, 1–9 (2021).
18. Sondak, C. F. et al. Carbon dioxide mitigation potential of seaweed aquaculture beds (SABs). *J. Appl. Phycol.* **29**, 2363–2373 (2017).
19. FAO. *The State of World Fisheries and Aquaculture 2022: Towards Blue Transformation* (Food and Agriculture Organization of the United Nations, 2022).
20. Bak, U. G., Mols-Mortensen, A. & Gregersen, O. Production method and cost of commercial-scale offshore cultivation of kelp in the Faroe Islands using multiple partial harvesting. *Algal Res.* **33**, 36–47 (2018).
21. Buck, B. H. et al. State of the art and challenges for offshore integrated multi-trophic aquaculture (IMTA). *Front. Mar. Sci.* **5**, 165 (2018).
22. Azevedo, I. C., Duarte, P. M., Marinho, G. S., Neumann, F. & Sousa-Pinto, I. Growth of *Saccharina latissima* (*Laminariales*, *phaeophyceae*) cultivated offshore under exposed conditions. *Phycologia* **58**, 504–515 (2019).
23. Navarrete, I. A. et al. Effects of depth-cycling on nutrient uptake and biomass production in the giant kelp *Macrocystis pyrifera*. *Renew. Sustain. Energy Rev.* **141**, 110747 (2021).
24. Solvang, T., Bale, E. S., Broch, O. J., Handå, A. & Alver, M. O. Automation concepts for industrial-scale production of seaweed. *Front. Mar. Sci.* **8**, 613093 (2021).
25. Chung, I. K., Beardall, J., Mehta, S., Sahoo, D. & Stojkovic, S. Using marine macroalgae for carbon sequestration: A critical appraisal. *J. Appl. Phycol.* **23**, 877–886 (2011).
26. Krause-Jensen, D. & Duarte, C. M. Substantial role of macroalgae in marine carbon sequestration. *Nat. Geosci.* **9**, 737–742 (2016).
27. Solidoro, C., Pecenik, G., Pastres, R., Franco, D. & Dejak, C. Modelling macroalgae (*Ulva rigida*) in the Venice lagoon: Model structure identification and first parameters estimation. *Ecol. Model.* **94**, 191–206 (1997).
28. Broch, O. J. & Slagstad, D. Modelling seasonal growth and composition of the kelp *Saccharina latissima*. *J. Appl. Phycol.* **24**, 759–776 (2012).
29. Hadley, S., Wild-Allen, K., Johnson, C. & Macleod, C. Modeling macroalgae growth and nutrient dynamics for integrated multi-trophic aquaculture. *J. Appl. Phycol.* **27**, 901–916 (2015).
30. Zhang, J., Wu, W., Ren, J. S. & Lin, F. A model for the growth of mariculture kelp *Saccharina japonica* in Sanggou Bay, China. *Aquac. Environ. Interact.* **8**, 273–283 (2016).
31. van der Molen, J et al. Modelling potential production of macroalgae farms in UK and Dutch coastal waters. *Biogeosciences* **15**, 1123–1147 (2018).
32. Wu, J., Keller, D. P. & Oschlies, A. Carbon dioxide removal via macroalgae open-ocean mariculture and sinking: An Earth system modeling study. *Earth Syst. Dynam.* **14**, 185–221 (2022).
33. Frieder, C. et al. A macroalgal cultivation modeling system (MACMODS): Evaluating the role of physical-biological coupling on nutrients and farm yield. *Front. Mar. Sci.* **9**, 214–232 (2022).
34. Roleda, M. Y. & Hurd, C. L. Seaweed nutrient physiology: application of concepts to aquaculture and bioremediation. *Phycologia* **58**, 552–562 (2019).
35. Atkinson, M. & Smith, S. C: N: P ratios of benthic marine plants 1. *Limnol. Oceanogr.* **28**, 568–574 (1983).
36. Martiny, A. C., Vrugt, J. A. & Lomas, M. W. Concentrations and ratios of particulate organic carbon, nitrogen, and phosphorus in the global ocean. *Sci. Data* **1**, 1–7 (2014).
37. Brzezinski, M. A. et al. Multiple sources and forms of nitrogen sustain year-round kelp growth: On the Inner Continental Shelf of the Santa Barbara Channel. *Oceanography* **26**, 114–123 (2013).
38. Smith, J. M., Brzezinski, M. A., Melack, J. M., Miller, R. J. & Reed, D. C. Urea as a source of nitrogen to giant kelp (*Macrocystis pyrifera*). *Limnol. Oceanogr. Lett.* **3**, 365–373 (2018).
39. Neish, I. C. Social and economic dimensions of carrageenan seaweed farming in the Indonesia. *Social and Economic Dimensions of Carrageenan Seaweed Farming.* Technical Paper No. 580 (FAO, 2013).
40. Hurtado, A. Q. Social and economic dimensions of carrageenan seaweed farming in the Philippines. *Social and Economic Dimensions of Carrageenan*

Seaweed Farming. Fisheries and Aquaculture Technical Paper No. 580 (FAO, 2013).
41. Camus, C., Infante, J. & Buschmann, A. H. Overview of 3 year precommercial seafarming of *Macrocystis pyrifera* along the Chilean coast. *Rev. Aquac.* **10**, 543–559 (2018).
42. Zhang, J. Seaweed industry in China. *Innovation Norway* (2018).
43. Brush, M. J. & Nixon, S. W. Modeling the role of macroalgae in a shallow sub-estuary of Narragansett Bay, RI (USA). *Ecol. Model.* **221**, 1065–1079 (2010).
44. He, Y., Xuan, J., Ding, R., Shen, H. & Zhou, F. Influence of suspended aquaculture on hydrodynamics and nutrient supply in the coastal Yellow Sea. *J. Geophys. Res. Biogeosci.* **127**, e2021JG006633 (2022).
45. Kelly, E. L., Cannon, A. L. & Smith, J. E. Environmental impacts and implications of tropical carrageenophyte seaweed farming. *Conserv. Biol.* **34**, 326–337 (2020).
46. Boyd, P. W. et al. Potential negative effects of ocean afforestation on offshore ecosystems. *Nat. Ecol. Evol.* **6**, 675–683 (2022).
47. DeAngelo, J. et al. Economic and biophysical limits to seaweed farming for climate change mitigation. *Nat. Plants* **9**, 45–57 (2022).
48. Behrenfeld, M. J. & Falkowski, P. G. Photosynthetic rates derived from satellite-based chlorophyll concentration. *Limnol. Oceanogr.* **42**, 1–20 (1997).
49. Siegel, D. et al. Global assessment of ocean carbon export by combining satellite observations and food-web models. *Global Biogeochem. Cycles* **28**, 181–196 (2014).
50. Littler, M. M. & Littler, D. S. The evolution of thallus form and survival strategies in benthic marine macroalgae: Field and laboratory tests of a functional form model. *Am. Nat.* **116**, 25–44 (1980).
51. Raven, J. Scaling the seas. *Plant Cell Environ.* **18**, 1090–1100 (1995).
52. Hurd, C., Harrison, P., Bischof, K. & Lobban, C. Seaweed thalli and cells. *Seaweed Ecol. Physiol.* **2**, 1–47 (2014).
53. Hurd, C., Harrison, P., Bischof, K. & Lobban, C. Nutrients. *Seaweed Ecol. Physiol.* **2**, 238–293 (2014).
54. Duffy, J. E. & Hay, M. E. Seaweed adaptations to herbivory. *Bioscience* **40**, 368–375 (1990).
55. Duarte, C. M. Nutrient concentration of aquatic plants: Patterns across species. *Limnol. Oceanogr.* **37**, 882–889 (1992).
56. Öberg, J. Primary production by macroalgae in Kattegat, estimated from monitoring data, seafloor properties, and model simulations. *Cont. Shelf Res.* **26**, 2415–2432 (2006).
57. Duarte, C. M. et al. Global estimates of the extent and production of macroalgal forests. *Global Ecol. Biogeogr.* **31**, 1422–1439 (2022).
58. Smith, S. Marine macrophytes as a global carbon sink. *Science* **211**, 838–840 (1981).
59. Rassweiler, A., Reed, D. C., Harrer, S. L. & Nelson, J. C. Improved estimates of net primary production, growth, and standing crop of *Macrocystis pyrifera* in Southern California. *Ecology* **99**, 2132(2018).
60. Zhu, G., Ebbing, A., Bouma, T. J. & Timmermans, K. R. Morphological and physiological plasticity of *Saccharina latissima* (*Phaeophyceae*) in response to different hydrodynamic conditions and nutrient availability. *J. Appl. Phycol.* **33**, 2471–2483 (2021).
61. Andersson, M., Schubert, H., Pedersén, M. & Snoeijs, P. Different patterns of carotenoid composition and photosynthesis acclimation in two tropical red algae. *Mar. Biol.* **149**, 653–665 (2006).
62. Freile-Pelegrín, Y. & Robledo, D. Carrageenan of *Eucheuma isiforme* (Solieriaceae, Rhodophyta) from Yucatán, México II. Seasonal variations in carrageenan and biochemical characteristics. *Bot. Mar.* **49**, 72–78 (2006).
63. Roberts, D. A., Paul, N. A., Dworjanyn, S. A., Bird, M. I. & de Nys, R. Biochar from commercially cultivated seaweed for soil amelioration. *Sci. Rep.* **5**, 1–6 (2015).
64. Martin, J., Ambrose Jr, R. & Wool, T. *WASP8 Macro Algae: Model Theory and User's Guide* https://www.epa.gov/sites/default/files/2018-05/documents/wasp-macroalgae_manual-v3.pdf (2018).
65. Trancoso, A. et al. Modelling macroalgae using a 3D hydrodynamic-ecological model in a shallow, temperate estuary. *Ecol. Model.* **187**, 232–246 (2005).
66. Hwang, E. K., Yotsukura, N., Pang, S. J., Su, L. & Shan, T. F. Seaweed breeding programs and progress in eastern Asian countries. *Phycologia* **58**, 484–495 (2019).
67. FAO. *The State of World Fisheries and Aquaculture 2022: Sustainability in Action* (Food and Agriculture Organization of the United Nations, 2020).
68. USGS. Map of croplands in the United States. https://www.usgs.gov/media/images/map-croplands-united-states#:~:text=The%20United%20States%20has%20166,180%20million%20hectares%20of%20croplands (2022).
69. Gao, G. et al. A review of existing and potential blue carbon contributions to climate change mitigation in the Anthropocene. *J. Appl. Ecol.* **59**, 1686–1699 (2022).
70. Bach, L. T. et al. Testing the climate intervention potential of ocean afforestation using the Great Atlantic *Sargassum* Belt. *Nat. Commun.* **12**, 1–10 (2021).
71. Berger, M., Kwiatkowski, L., Ho, D. T. & Bopp, L. Ocean dynamics and biological feedbacks limit the potential of macroalgae carbon dioxide removal. *Environ. Res. Lett.* **18**, 024039(2023).
72. Ren, J. S., Stenton-Dozey, J., Plew, D. R., Fang, J. & Gall, M. An ecosystem model for optimising production in integrated multitrophic aquaculture systems. *Ecol. Model.* **246**, 34–46 (2012).
73. Duarte, P. & Ferreira, J. A model for the simulation of macroalgal population dynamics and productivity. *Ecol. Model.* **98**, 199–214 (1997).
74. Kambey, C. S. et al. Seaweed aquaculture: A preliminary assessment of biosecurity measures for controlling the ice-ice syndrome and pest outbreaks of a *Kappaphycus* farm. *J. Appl. Phycol.* **33**, 3179–3197 (2021).
75. Smith, C. R., De Leo, F. C., Bernardino, A. F., Sweetman, A. K. & Arbizu, P. M. Abyssal food limitation, ecosystem structure and climate change. *Trends Ecol. Evol.* **23**, 518–528 (2008).
76. Smith, C. R. et al. Latitudinal variations in benthic processes in the abyssal equatorial Pacific: control by biogenic particle flux. *Deep Sea Res. Part II Top. Stud. Oceanogr.* **44**, 2295–2317 (1997).
77. Nomaki, H. et al. In situ experimental evidences for responses of abyssal benthic biota to shifts in phytodetritus compositions linked to global climate change. *Glob. Change Biol.* **27**, 6139–6155 (2021).
78. Jarvis, B. M. et al. Modeling spatiotemporal patterns of ecosystem metabolism and organic carbon dynamics affecting hypoxia on the Louisiana Continental Shelf. *J. Geophys. Res. Oceans* **125**, e2019JC015630 (2020).
79. Yu, L., Fennel, K., Laurent, A., Murrell, M. C. & Lehrter, J. C. Numerical analysis of the primary processes controlling oxygen dynamics on the Louisiana shelf. *Biogeosciences* **12**, 2063–2076 (2015).
80. Ricart, A. M. et al. Sinking seaweed in the deep ocean for carbon neutrality is ahead of science and beyond the ethics. *Environ. Res. Lett.* **17**, 081003 (2022).
81. Droop, M. R. Some thoughts on nutrient limitation in algae. *J. Phycology* **9**, 264–272 (1973).
82. Moore, J. K., Doney, S. C., Glover, D. M. & Fung, I. Y. Iron cycling and nutrient-limitation patterns in surface waters of the World Ocean. *Deep Sea Res. Part II Top. Stud. Oceanogr.* **49**, 463–507 (2001).
83. Pessarrodona, A., Moore, P. J., Sayer, M. D. & Smale, D. A. Carbon assimilation and transfer through kelp forests in the NE Atlantic is diminished under a warmer ocean climate. *Glob. Change Biol.* **24**, 4386–4398 (2018).
84. Visch, W., Nylund, G. M. & Pavia, H. Growth and biofouling in kelp aquaculture (*Saccharina latissima*): The effect of location and wave exposure. *J. Appl. Phycol.* **32**, 3199–3209 (2020).
85. Fram, J. P. et al. Physical pathways and utilization of nitrate supply to the giant kelp, *Macrocystis pyrifera*. *Limnol. Oceanogr.* **53**, 1589–1603 (2008).
86. Sanford, L. P. & Crawford, S. M. Mass transfer versus kinetic control of uptake across solid-water boundaries. *Limnol. Oceanogr.* **45**, 1180–1186 (2000).
87. Stevens, C. L. & Hurd, C. L. Boundary-layers around bladed aquatic macrophytes. *Hydrobiologia* **346**, 119–128 (1997).
88. Yuan-Hui, L. & Gregory, S. Diffusion of ions in sea water and in deep-sea sediments. *Geochim. Cosmochim. Acta* **38**, 703–714 (1974).
89. Dade, W. B. Near-bed turbulence and hydrodynamic control of diffusional mass transfer at the sea floor. *Limnol. Oceanogr.* **38**, 52–69 (1993).
90. Stevens, C. L., Hurd, C. L. & Isachsen, P. E. Modelling of diffusion boundary-layers in subtidal macroalgal canopies: The response to waves and currents. *Aquat. Sci.* **65**, 81–91 (2003).
91. Huang, I., Rominger, J. & Nepf, H. The motion of kelp blades and the surface renewal model. *Limnol. Oceanogr.* **56**, 1453–1462 (2011).
92. Xiao, X. et al. Resource (light and nitrogen) and density-dependence of seaweed growth. *Front. Mar. Sci.* **6**, 618 (2019).
93. Cerco, C. & Cole, T. M. *User's Guide to the CE-QUAL-ICM Three-dimensional Eutrophication Model: Release version 1.0*. Report No. EL-95-15 (Environmental Laboratory, 1995).
94. Di Toro, D. M., O'Conno, D. J. & Thomann, R. V. A dynamic model of the phytoplankton population in the Sacramento-San Joaquin Delta. *Adv. Chem.* **106**, 131–180 (1971).
95. Long, M. C. et al. Simulations with the Marine Biogeochemistry Library (MARBL). *J. Adv. Model. Earth Syst.* **13**, e2021MS002647 (2021).
96. MARBL Developers. *MARBL Documentation: Release CESM 2.1*. NCAR. https://buildmedia.readthedocs.org/media/pdf/marbl/latest/marbl.pdf (n.d.).
97. Duarte, P. & Ferreira, J. A methodology for parameter estimation in seaweed productivity modelling. In *Fourteenth International Seaweed Symposium* 183–189 (Springer, 1993).
98. Rodriguez, G. E., Rassweiler, A., Reed, D. C. & Holbrook, S. J. The importance of progressive senescence in the biomass dynamics of giant kelp (*Macrocystis pyrifera*). *Ecology* **94**, 1848–1858 (2013).
99. Oregon State University Ocean Productivity Group. 1080 x 2160 x 8-day input data. https://sites.science.oregonstate.edu/ocean.productivity/1080.by.2160.8day.inputData.php (n.d.).
100. Oregon State University Ocean Productivity Group. 1080 x 2160 x 8-day hdf files. http://orca.science.oregonstate.edu/1080.by.2160.8day.hdf.vgpm.m.chl.m.sst.php (n.d.).
101. Wallcraft, A., Metzger, E. & Carroll, S. *Software Design Description for the Hybrid Coordinate Ocean Model (HYCOM), Version 2.2*. Tech. Rep. (Naval Research Lab Stennis Space Center, 2009).

102. Hybrid Coordinate Ocean Model (HYCOM) Data Assimilative System. Global Ocean Forecast System 3.1 (GOFS 3.1) Analysis. https://www.hycom.org/dataserver/gofs-3pt1/analysis (n.d.).
103. Cummings, J. A. Operational multivariate ocean data assimilation. *Q. J. R. Meteorol. Soc. A* **131**, 3583–3604 (2005).
104. Hersbach, H. et al. The ERA5 global reanalysis. *Q. J. R. Meteorol. Soc.* **146**, 1999–2049 (2020).
105. Hersbach, H. et al. ERA5 hourly data on single levels from 1940 to present. Copernicus Climate Change Service (C3S) Climate Data Store (CDS). (2018).
106. Hurrell, J. W. et al. The Community Earth System Model: a framework for collaborative research. *Bull. Am. Meteorol. Soc.* **94**, 1339–1360 (2013).
107. Harrison, C. S., Long, M. C., Lovenduski, N. S. & Moore, J. K. Mesoscale effects on carbon export: A global perspective. *Glob. Biogeochem. Cycles* **32**, 680–703 (2018).
108. Long, M. C. & Saenz, B. T. Nitrate flux and inventory from high-resolution CESM CORE-Normal-Year integration (2023).
109. Ferdouse, F., Holdt, S. L., Smith, R., Murúa, P. & Yang, Z. The global status of seaweed production, trade and utilization. *Globefish Res. Programme* **124**, I (2018).
110. Tahiluddin, A. B., Nuñal, S. N. & Santander-de Leon, S. M. S. Inorganic nutrient enrichment of seaweed *Kappaphycus*: Farmers' practices and effects on growth and ice-ice disease occurrence. *Regional Studies in Marine Science* **55**, 102593 (2022).
111. Wang, X. et al. Economically important red algae resources along the Chinese coast: History, status, and prospects for their utilization. *Algal Res.* **46**, 101817 (2020).
112. Marinho, G. S., Holdt, S. L., Birkeland, M. J. & Angelidaki, I. Commercial cultivation and bioremediation potential of sugar kelp, *Saccharina latissima*, in Danish waters. *J. Appl. Phycol.* **27**, 1963–1973 (2015).
113. Msuya, F. E. et al. A comparative economic analysis of two seaweed farming methods in Tanzania. *The Sustainable Coastal Communities and Ecosystems Program. Coastal Resources Center, University of Rhode Island and the Western Indian Ocean Marine Science Association* (2007).
114. McPhee-Shaw, E. E. et al. Mechanisms for nutrient delivery to the inner shelf: Observations from the Santa Barbara Channel. *Limnol. Oceanogr.* **52**, 1748–1766 (2007).
115. Largo, D. B., Fukami, K., Nishijima, T. & Ohno, M. Laboratory-induced development of the ice-ice disease of the farmed red algae *Kappaphycus alvarezii* and *Eucheuma denticulatum* (Solieriaceae, Gigartinales, Rhodophyta). *J. Appl. Phycol.* **7**, 539–543 (1995).
116. Largo, D. B., Msuya, F. E. & Menezes, A. Understanding diseases and control in seaweed farming in Zanzibar. *FAO Fisheries and Aquaculture Technical Paper* 0_1–49 (FAO, 2020).

Acknowledgements

This work was funded by the ClimateWorks Foundation (#UCI-21-1763). Additionally, I.B.A.-S. was supported by NSF grant #OCE-2022927 and K.A.D. was supported by DOE/ARPA-E grant #DE-AR0000920. We appreciate the valuable feedback provided by the four reviewers as well as the contributions of Dr. Loretta Roberson (MBL).

Author contributions

K.A.D., C.A.F., B.T.S., and S.J.D. conceived the work. I.B.A.-S. wrote the first draft of the manuscript. I.B.A.-S., C.A.F., and B.T.S. designed and coded G-MACMODS with the help of K.A.D. B.T.S. downloaded and interpolated the environmental forcing data. M.C.L. provided the nitrate data. M.C.L., S.J.D., and J.D. provided context for the atmospheric and economic implications of the work. All authors contributed to interpreting the results, as well as framing and revising the paper.

Competing interests

The authors declare no competing interests.

Additional information

Supplementary information The online version contains supplementary material available at https://doi.org/10.1038/s43247-023-00833-2.

Correspondence and requests for materials should be addressed to Isabella B. Arzeno-Soltero or Kristen A. Davis.

Peer review information *Communications Earth & Environment* thanks John Beardall, Meiron Zollmann and the other, anonymous, reviewer(s) for their contribution to the peer review of this work. Primary Handling Editors: Christopher Cornwall, Joe Aslin and Clare Davis. Peer reviewer reports are available.